SUPPORTING INFORMATION

High-valent oxovanadium metallosupramolecular species as catalysts for the oxidation of benzyl alcohol derivatives

Edi Topić,[a] Josipa Sarjanović,[a] Danijela Musija,[b] Mirna Mandarić,[a] Tomica Hrenar,[a] Jana Pisk,*[a] and Višnja Vrdoljak*[a]

Table of Contents

[a] *University of Zagreb, Faculty of Science, Department of Chemistry, Horvatovac 102a, 10000 Zagreb, Croatia; E-mail: visnja.vrdoljak@chem.pmf.hr*
[b] *University of Zagreb, School of Medicine, Department of Chemistry and Biochemistry, Šalata 3, 10000 Zagreb, Croatia.*

1. Characterization of compounds

Elemental analyses (C, H, and N) were performed by the Analytical Services Laboratory of Rudjer Bošković Institute, Zagreb.

Powder X-ray diffraction (PXRD) data were collected on a Malvern Panalytical Aeris diffractometer in the Bragg-Brentano geometry using CuK_α radiation (λ = 1.5406 Å). Powder patterns were collected at room temperature in the region between 5° and 40° (2θ). The data were collected and visualized using the Malvern Panalytical HighScore Software Suite.[1]

Single crystal diffraction (SCXRD)

High-quality single crystals were grown in a way described in the manuscript. Diffracted intensities were collected on Rigaku XtaLAB Synergy-S diffractometer equipped with Dualflex source (CuKα radiation, λ = 1.54184 Å), and HyPix detector using ω-scans. The crystals were kept at 170 K during data collection. Data were prepared using the CrysAlis program package.[2] The structures were solved with dual space methods using SHELXT.[3] The refinement procedure by full-matrix least-squares methods based on F^2 values against all reflections included anisotropic displacement parameters for all non-H atoms. Hydrogen atoms bound to carbon atoms were placed in geometrically idealized positions and refined using the riding model with U_{iso} = 1.2U_{eq} of the connected carbon atom or as ideal CH_3 groups with U_{iso} = 1.5U_{eq}. Where possible, hydrogen atoms attached to heteroatoms were located in the difference Fourier maps at the final stages of the refinement procedure. Disorder of alkoxy chains of **1β, 2β** and **5β** was modelled in two orientations based on peaks in difference Fourier map. Void volume electron density in **1t**, **1β, 2β** and **5β** was modelled using solvent mask as implemented in Olex2. All refinements were performed using SHELXL.[4] The SHELX programs operated within the Olex2 suite.[5] Geometrical calculations and molecular graphics were done with Platon[6] and Mercury.[7] CCDC 2367532-2367538 contain the supplementary crystallographic data for this paper. These data can be obtained free of charge via http://www.ccdc.cam.ac.uk/conts/retrieving.html (or from the Cambridge Crystallographic Data Centre, 12, Union Road, Cambridge CB2 1EZ, UK; fax: +44 1223 336033).

UV-Vis spectroscopy

UV-Vis measurements were carried out using a Varian Cary Bio 100 spectrophotometer with 1-cm quartz cuvettes. The UV-Vis spectra of H_2SIH and complexes **1t** and **1**–**6** were recorded in methanol and acetonitrile at room temperature immediately after solution preparation. All compounds, except complex **6**, were dissolved in methanol or acetonitrile within minutes using ultrasound. The concentrations used were 6.0 × 10^{-5} mol dm^{-3} for H_2SIH and complexes **1**–**5**, 1.5 × 10^{-5} mol dm^{-3} for complex **1t**, and below 3 × 10^{-5} mol dm^{-3} for complex **6** due to incomplete dissolution.

Nuclear magnetic resonance spectra (^{1}H, APT, gHMQC and gHMBC NMR) were acquired on a Bruker Avance 600 NMR spectrometer using a C/H dual 5 mm probe and z-gradient accessories at 298K in CD_3OD or $CDCl_3$ and TMS as the internal standard.

Attenuated Total Reflectance Infrared spectra (ATR-IR) were recorded on a Perkin Elmer Spectrum One spectrometer fitted with an ATR reluctance attachment. Spectra were collected in the 4000–450 cm^{-1} range on a diamond window.

Differential scanning calorimetry (DSC) method was used for getting information about the purity of hydrazone. Measurement was performed under the nitrogen stream (10 mL min^{-1}) on the TA Discovery DSC 25 instrument using Tzero aluminium pans and lids. The heating rate was 10 K min^{-1} in the

temperature range from 25 to 400 °C. The result was evaluated using the TA Instruments Trios (v5.1.1.46572) software.

Thermogravimetric analyses (TGA) were performed on a Mettler-Toledo TG/DSC 3+ Stare System thermobalance using open alumina crucibles under an oxygen atmosphere in the temperature range from 25 to 600 °C. All experiments were recorded with a heating rate of 5 °C min^{-1} in a dynamic atmosphere with a flow rate of 10 mL min^{-1}. The results of TGA and experiments were evaluated using the Mettler STARe software.

Fourier Transform Infrared spectra (FTIR) of the gaseous products evolved during thermal decomposition of the complexes were recorded with the use of the thermobalance coupled online with the Nicolet iS50 FT-IR spectrometer (Thermo Scientific) by a transfer line heated at 200 °C. FTIR spectra were recorded in the range of 4000–400 cm^{-1} with a resolution of 4 cm^{-1}.

Catalytic investigation

The catalytic oxidation of alcohols was monitored using gas chromatography (GC) on an Agilent 8860 chromatograph (Agilent Technologies, Santa Clara, CA, USA) equipped with a flame ionization detector (FID) and an HP-5 column (30 m × 0.320 mm × 0.25 μm). Quantification of reaction parameters was achieved through calibration curves generated from authentic standards of the reactants and products. The conversion of alcohols to their respective aldehydes was calculated relative to internal standards, including biphenyl for benzyl alcohol, acetophenone for 2-nitro and 2-chlorobenzyl alcohol, and dodecane for 2-methylbenzyl alcohol. Calibration curve correlation coefficients (R^2) were consistently high at 0.9999, confirming the accuracy of the quantification.

1.1. PXRD

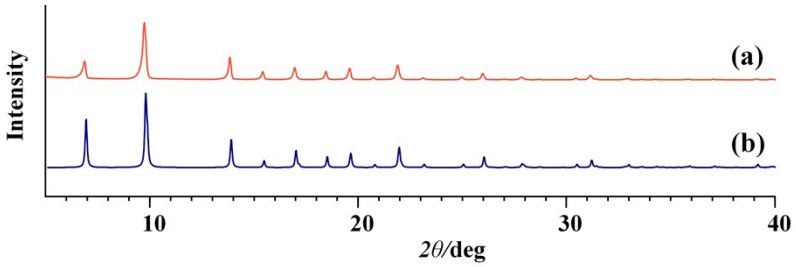

Fig. S1 Powder X-ray diffraction patterns of (a) tetranuclear assembly $[VO(SIH)(OCH_3)]_4 \cdot 4CH_3OH$ (**1t**·$4CH_3OH$) obtained by reaction of NH_4VO_3 with H_2SIH in CH_3OH; (b) $[VO(SIH)(OCH_3)]_4 \cdot 4CH_3OH$ (**1t**·$4CH_3OH$) calculated from the X-ray single-crystal structure.

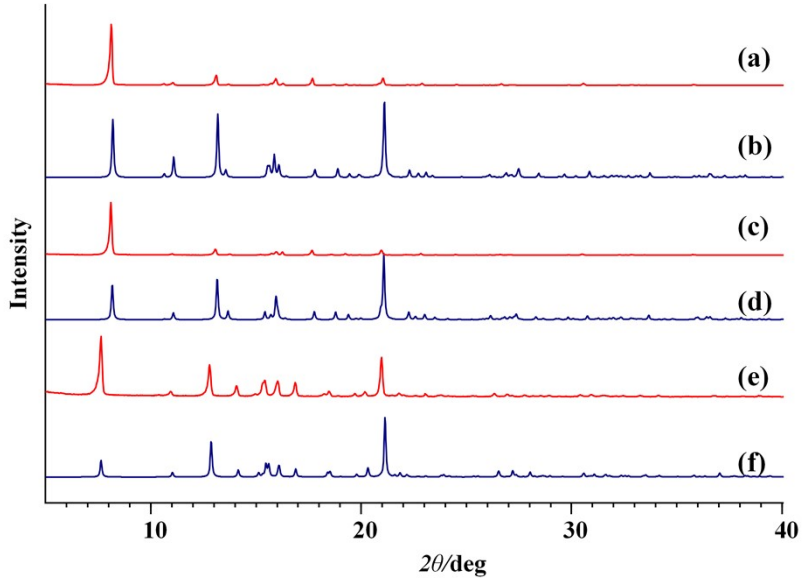

Fig. S2 Powder X-ray diffraction patterns of polynuclear assemblies $[VO(SIH)(OR)]_n$ belonging to **α** series: (a and b) R = OC_2H_5 (**2α**); (c and d) R = OC_3H_7 (**3α**), (e and f) R = OC_4H_9 (**4α**). The red lines indicate those of prepared samples, while the blue lines indicate those calculated from the X-ray single-crystal structures of the corresponding samples.

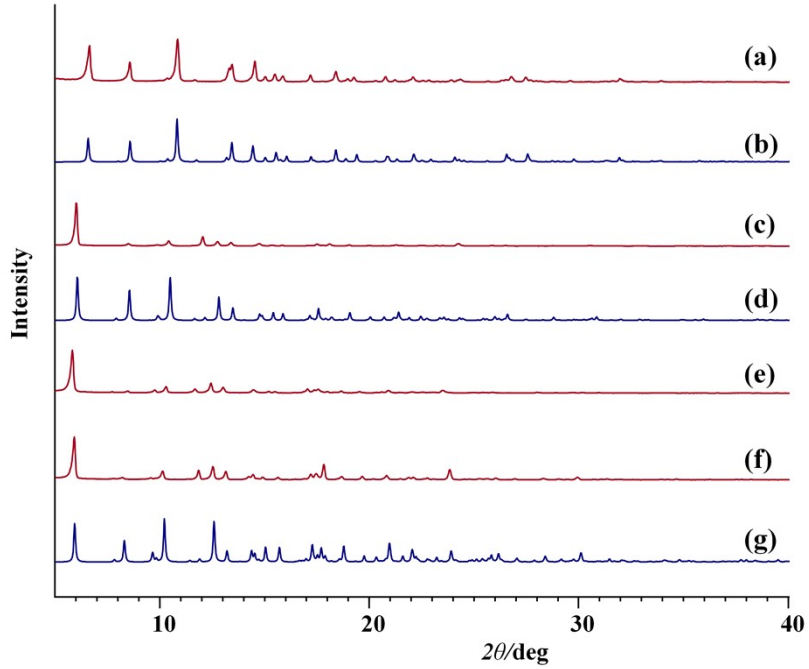

Fig. S3 Powder X-ray diffraction patterns of polynuclear assemblies $[VO(SIH)(OR)]_n$ belonging to **α** series: (a and b) R =OCH_3 (**1β** ·0.25CH_3OH); (c and d) R = OC_2H_5 (**2β**·0.25C_2H_5OH), (e) R = OC_4H_9 (**4β**); (f and g) R = OC_5H_{10} (**5β**). The red lines indicate those of prepared samples, while the blue lines indicate those calculated from the X-ray single-crystal structures of the corresponding samples.

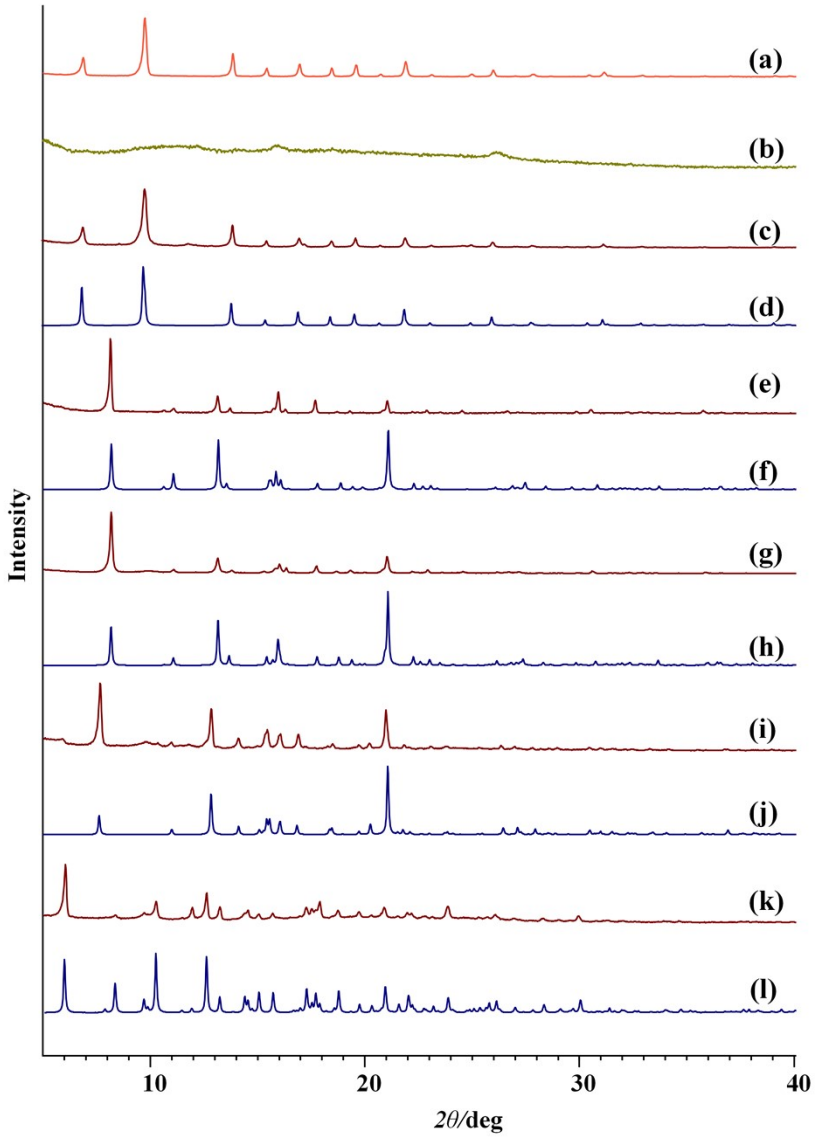

Fig. S4 Powder X-ray diffraction patterns of
(a) $[VO(SIH)(OCH_3)]_4 \cdot 4CH_3OH$ (**1t**·$4CH_3OH$) obtained by reaction of NH_4VO_3 with H_2SIH in CH_3OH;
(b) thermally activated complex $[VO(SIH)]_x$ obtained by heating of **1t**·$4CH_3OH$ for 1 hour at 165 °C;
(c) sample obtained upon an immersion of $[VO(SIH)]_x$ in methanol for one week;
(d) $[VO(SIH)(OCH_3)]_4 \cdot 4CH_3OH$ (**1t**·$4CH_3OH$) calculated from the X-ray single-crystal structure;
(e) sample obtained upon an immersion of $[VO(SIH)]_x$ in ethanol for one week;
(f) $[VO(SIH)(OC_2H_5)]_n \cdot 0.25CH_3OH$ (**2α**) calculated from the X-ray single-crystal structure;
(g) sample obtained upon an immersion of $[VO(SIH)]_x$ in propanol for one week;
(h) $[VO(SIH)(OC_3H_7)]_n$ (**3α**) calculated from the X-ray single-crystal structure;
(i) sample obtained upon an immersion of $[VO(SIH)]_x$ in butanol for one week;
(j) $[VO(SIH)(OC_4H_9)]_n$ (**4α**) calculated from the X-ray single-crystal structure;
(k) sample obtained upon an immersion of $[VO(SIH)]_x$ in pentanol for one week;
(l) $[VO(SIH)(OC_4H_9)]_n$ (**5β**) calculated from the X-ray single-crystal structure;

1.2. SCXRD

Table S1 Experimental and crystallographic data for **α** polymorphs of [VO(OR)(SIH)] polymers

Identifier	**2α**	**3α**	**4α**
Empirical formula	$C_{15}H_{14}N_3O_4V$	$C_{16}H_{16}N_3O_4V$	$C_{17}H_{18}N_3O_4V$
M_r	351.23	365.26	379.28
T/K	169.99(10)	169.99(10)	169.99(10)
Crystal system	orthorhombic, dark red irregular	orthorhombic, brown plate	orthorhombic, orange irregular
Space group	*P b c a*	*P b c a*	*P b c a*
a/Å	13.05222(6)	12.9499(3)	12.5068(2)
b/Å	11.39032(5)	11.4867(3)	11.70940(10)
c/Å	21.55450(11)	21.6234(5)	23.1275(3)
α/°	90	90	90
β/°	90	90	90
γ/°	90	90	90
V/Å^3	3204.49(2)	3216.52(13)	3386.96(8)
Z	8	8	8
ρ_{calc}/g cm^{-3}	1.456	1.509	1.488
μ/mm^{-1}	5.391	5.393	5.143

$F(000)$	1440	1504	1568
Crystal size/mm^3	0.665×0.14×0.11	0.26×0.05×0.02	0.195×0.078×0.042
Radiation	CuKα (λ = 1.54184Å)	CuKα (λ = 1.54184Å)	CuKα (λ = 1.54184Å)
2Θ range/°	8.204 to 155.53	8.178 to 155.356	7.646 to 155.626
Index ranges	$-16 \le h \le 16$, $-14 \le k \le 14$, $-23 \le l \le 27$	$-8 \le h \le 16$, $-14 \le k \le 14$, $-26 \le l \le 27$	$-15 \le h \le 14$, $-14 \le k \le 14$, $-29 \le l \le 29$
Reflections collected	127302	16891	24059
Independent reflections	3412 [R_{int} = 1.44%, R_{sigma} = 5.88 %]	3389 [R_{int} = 3.33%, R_{sigma} = 3.87 %]	3604 [R_{int} = 2.82%, R_{sigma} = 3.79 %]
Data/restraints/parameters	3412/-/210	3389/-/218	3604/-/227
g_1, g_2 in w[a]	0.0437, 1.5078	0.0479, 2.2125	0.0704, 3.7488
Goodness–of–fit on F^2, S[b]	1.096	1.068	1.077
Final R and wR[c] values [$I \ge 2\sigma(I)$]	R_1 = 2.87%, wR_2 = 8.17%	R_1 = 3.77%, wR_2 = 9.95%	R_1 = 4.76%, wR_2 = 12.93%
Final R and wR[c] values [all data]	R_1 = 2.89%, wR_2 = 8.2%	R_1 = 4.2%, wR_2 = 10.24%	R_1 = 5.13%, wR_2 = 13.3%
Largest diff. peak/hole / e Å^{-3}	0.545/–0.339	0.620/–0.372	1.317/–0.558

[a] $w = 1/[\sigma F_o^2 + (g_1P)^2 + g_2P]$ where $P = (F_o^2 + 2F_c^2)/3$

[b] $S = \{\Sigma[w(F_o^2 - F_c^2)2]/(N_r - N_p)\}^{1/2}$ where N_r = number of independent reflections, N_p = number of refined parameters.

[c] $R = \Sigma||F_o| - |F_c|/\Sigma|F_o|$; $wR = \{\Sigma[w(F_o^2 - F_c^2)2]/\Sigma[w(F_o^2)2]\}^{1/2}$

Table S2 Experimental and crystallographic data for **β** polymorphs of [VO(OR)(SIH)] polymers and **1t**·4CH_3OH tetramer

Identifier	**1β**·0.25CH_3OH	**1t**·4CH_3OH	**2β**·0.25C_2H_5OH	**5β**
Empirical formula	$C_{57}H_{52}N_{12}O_{17}V_4$	$C_{15}H_{16}N_3O_5V$	$C_{31\cdot34}H_{26}N_6O_{8\cdot50}V_2$	$C_{35\cdot67}H_{28\cdot50}N_6O_8V_2$
M_r	690.43	369.25	724.60	771.03
T/K	169.98(10)	170(2)	293(2)	170(2)
Crystal system	orthorhombic, brown plate	tetragonal, yellow block	orthorhombic, brown plate	orthorhombic, brown block
Space group	*I b c a*	*I* –4	*I b c a*	*I b c a*
a/Å	22.0687(2)	18.1755(4)	20.6605(9)	21.2703(3)
b/Å	20.5886(2)	18.1755(4)	22.3137(8)	29.7362(4)
c/Å	26.8420(3)	10.3739(4)	29.1125(15)	22.5536(4)
α/°	90	90	90	90
β/°	90	90	90	90
γ/°	90	90	90	90
V/Å^3	12196.0(2)	3427.0(2)	13421.2(10)	14265.1(4)
Z	16	8	16	16
ρ_{calc}/g cm^{-3}	1.504	1.431	1.434	1.436
μ/mm^{-1}	5.668	5.112	5.181	4.901
F(000)	5648	1520	5921	6312
Crystal size/mm^3	0.227×0.19×0.051	0.09×0.06×0.05	0.32×0.02×0.02	0.05×0.03×0.02
Radiation	CuKα (λ = 1.54184Å)	CuKα (λ = 1.54184Å)	CuKα (λ = 1.54184Å)	CuKα (λ = 1.54184Å)

2Θ range/°	8.012 to 155.45	9.818 to 155.094	7.924 to 154.864	8.246 to 155.516
Index ranges	$-24 \le h \le 27$, $-19 \le k \le 26$, $-33 \le l \le 34$	$-22 \le h \le 22$, $-19 \le k \le 23$, $-13 \le l \le 13$	$-24 \le h \le 26$, $-28 \le k \le 26$, $-35 \le l \le 35$	$-26 \le h \le 20$, $-37 \le k \le 37$, $-28 \le l \le 28$
Reflections collected	34430	17514	86108	33047
Independent reflections	6412 [R_{int} = 2.55%, R_{sigma} = 3.15 %]	3558 [R_{int} = 4.21%, R_{sigma} = 5.22 %]	6996 [R_{int} = 4.66%, R_{sigma} = 12.28 %]	7431 [R_{int} = 4.93%, R_{sigma} = 8.63 %]
Data/restraints/parameters	6412/-/409	3558/-/200	6996/-/428	7431/-/494
g_1, g_2 in w[a]	0.0547, 11.9058	0.0506, 1.9758	0.0868, 7.4950	0.1305, 16.8622
Goodness–of–fit on F^2, S[b]	1.092	1.074	1.023	1.050
Final R and wR[c] values [$I \ge 2\sigma(I)$]	R_1 = 3.52%, wR_2 = 9.99%	R_1 = 3.81%, wR_2 = 9.87%	R_1 = 5.77%, wR_2 = 14.71%	R_1 = 6.78%, wR_2 = 19.09%
Final R and wR[c] values [all data]	R_1 = 3.77%, wR_2 = 10.18%	R_1 = 4.18%, wR_2 = 10.28%	R_1 = 9.49%, wR_2 = 16.96%	R_1 = 8.88%, wR_2 = 20.74%
Largest diff. peak/hole / e Å^{-3}	0.348/–0.474	0.160/–0.291	0.581/–0.413	0.916/–0.781
Flack parameter	-	0.005(4)	-	-

[a] $w = 1/[\sigma F_o^2 + (g_1P)^2 + g_2P]$ where $P = (F_o^2 + 2F_c^2)/3$

[b] $S = \{\Sigma[w(F_o^2 - F_c^2)2]/(N_r - N_p)\}^{1/2}$ where N_r = number of independent reflections, N_p = number of refined parameters.

[c] $R = \Sigma||F_o| - |F_c|/\Sigma|F_o|$; $wR = \{\Sigma[w(F_o^2 - F_c^2)2]/\Sigma[w(F_o^2)2]\}^{1/2}$

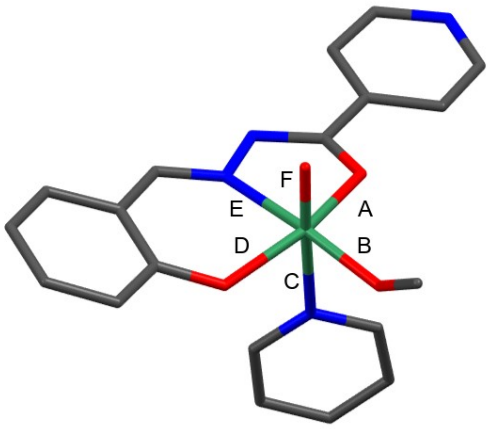

	2α	3α	4α	1t	1β	2β	5β
A	1.965	1.962	1.970	1.868	1.987	1.968	1.969
B	1.766	1.761	1.765	1.774	1.778	1.766	1.769
C	2.419	2.442	2.475	2.380	2.430	2.457	2.418
D	1.866	1.864	1.852	1.963	1.847	1.847	1.856
E	2.136	2.135	2.131	2.126	2.118	2.125	2.117
F	1.589	1.589	1.589	1.585	1.594	1.587	1.590

Fig. S5 Bond lengths in the coordination environment of the vanadium ion. Bond length standard deviations are omitted for clarity, and can be found in respective CIF files.

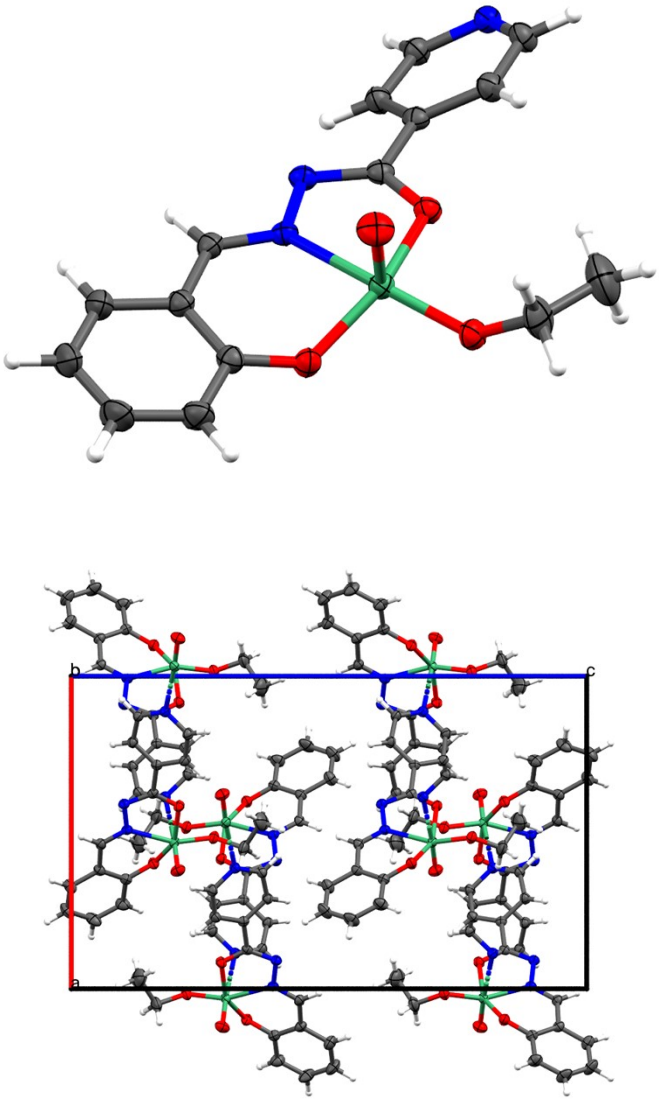

(a) 2α

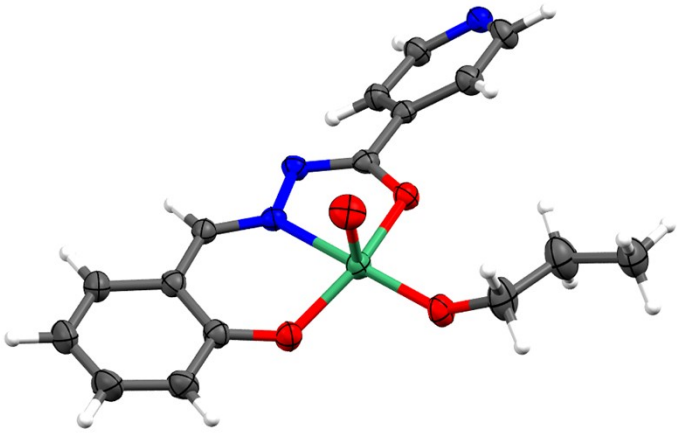

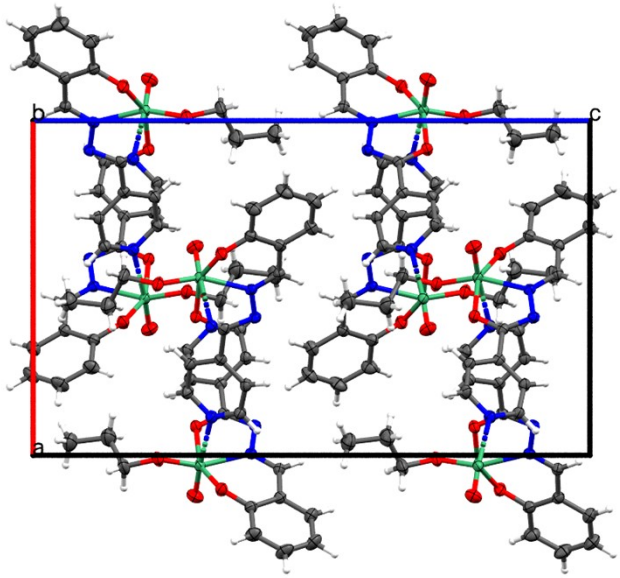

(b) 3α

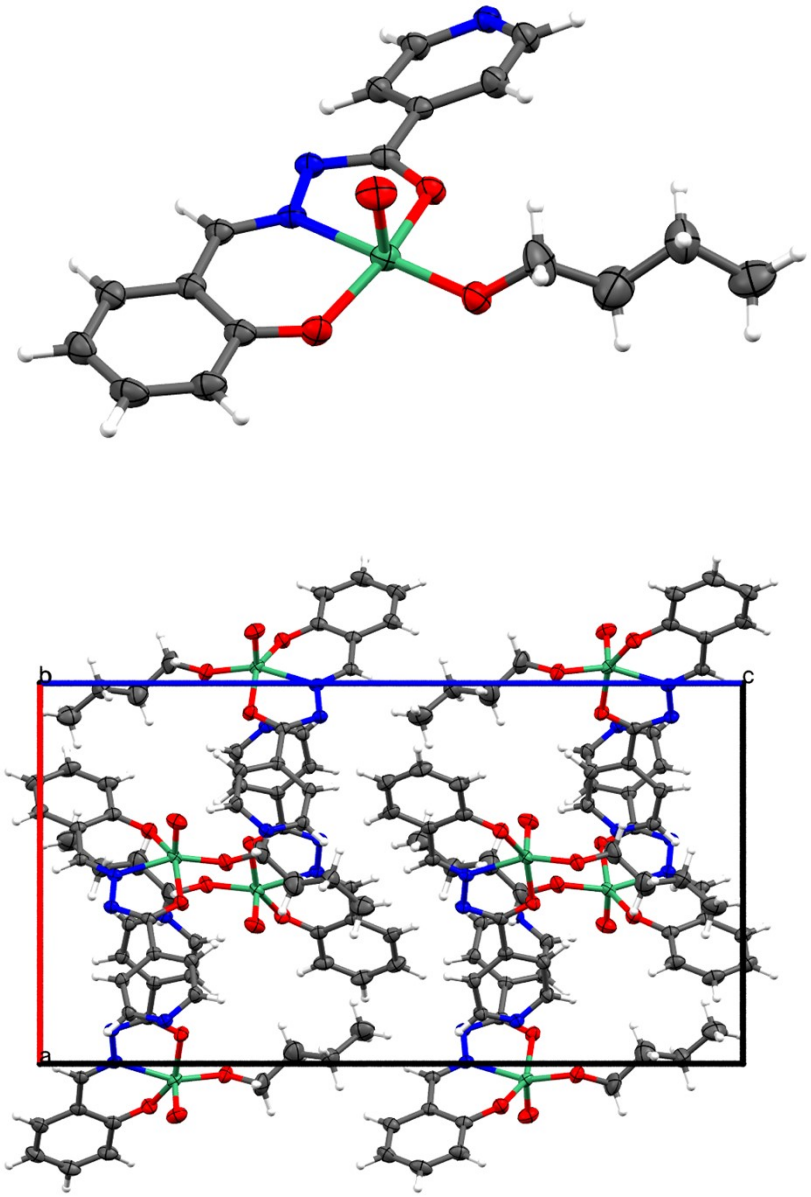

(c) 4α

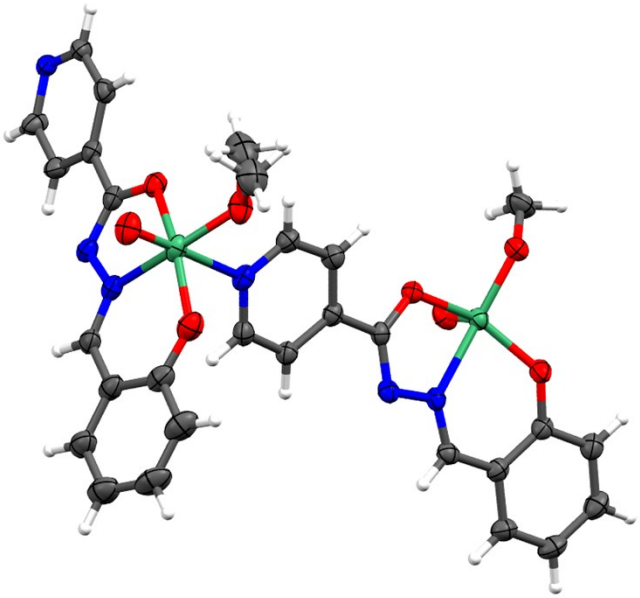

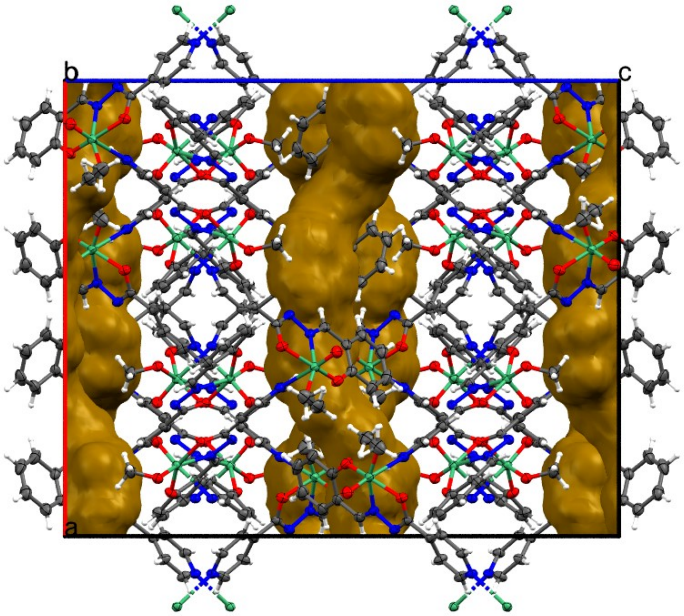

(d) 1β

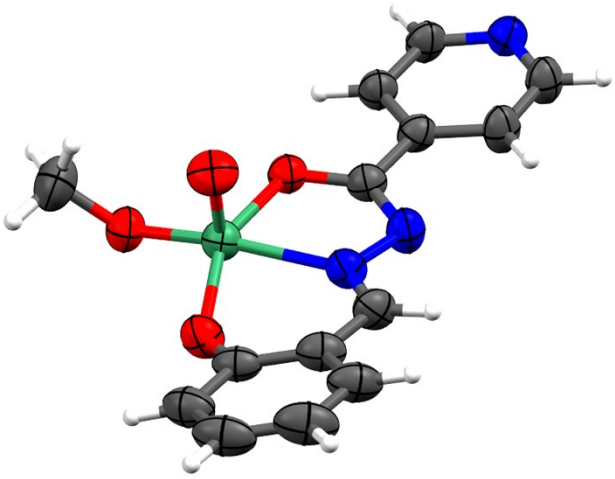

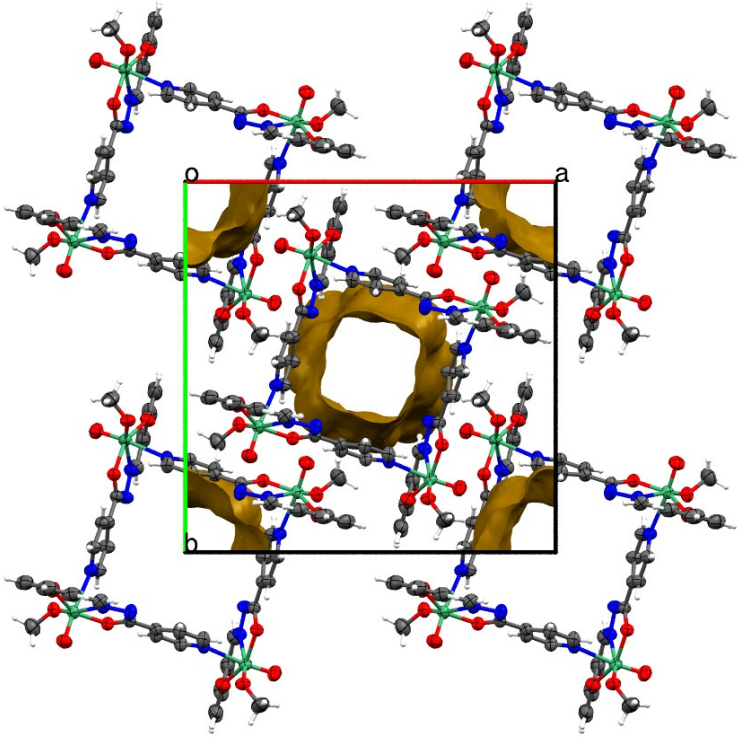

(e) 1t

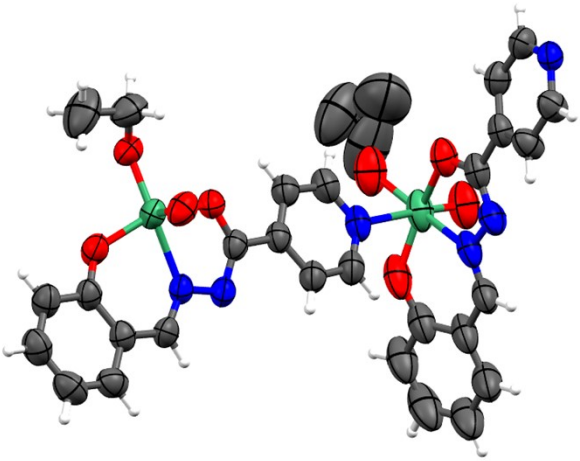

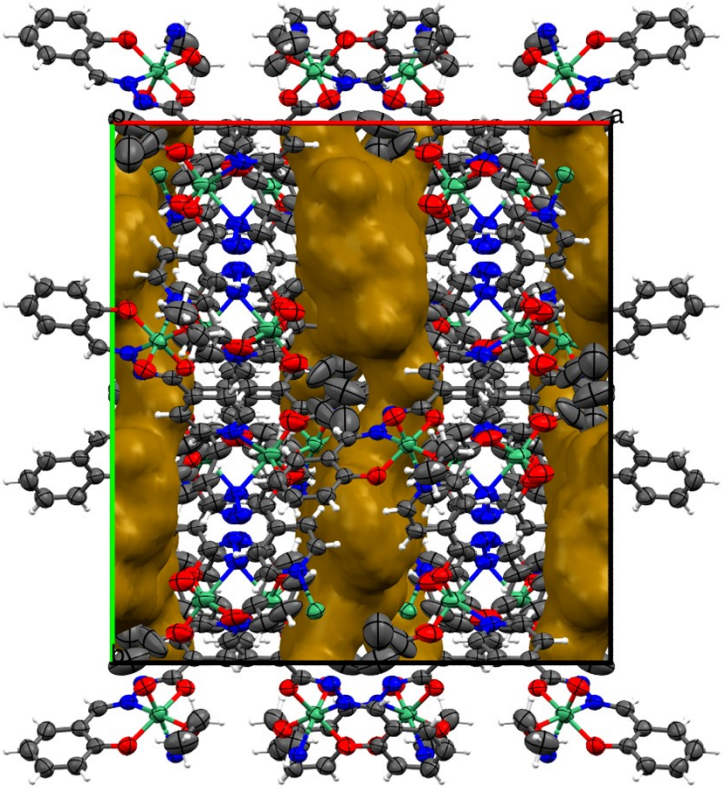

(f) 2β

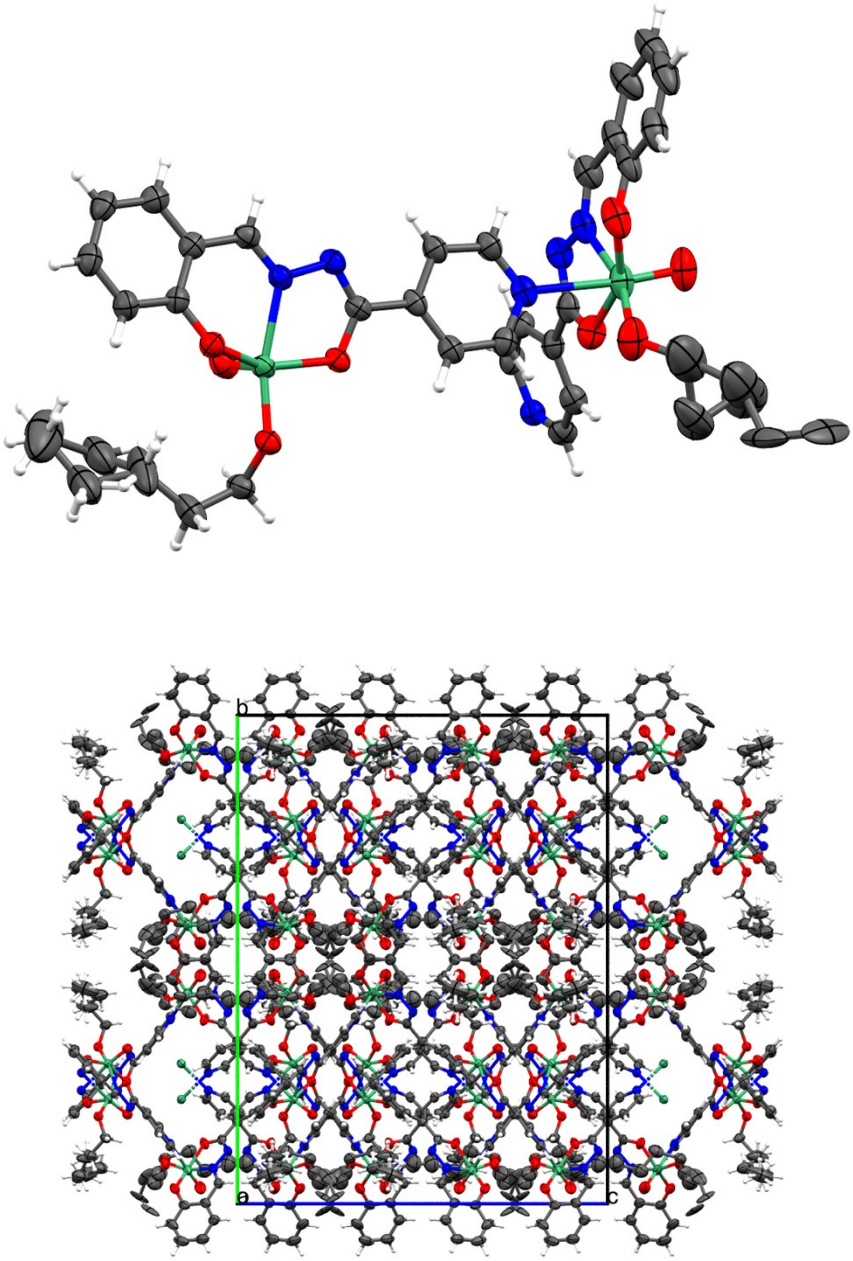

(g) 5β

Fig. S6 Asymmetric unit (top) and packing of molecules/polymers (bottom) for compounds characterized in this work. Atoms are shown as thermal ellipsiods at 50% probability level. Where applicable, void space is enclosed in yellow surface.

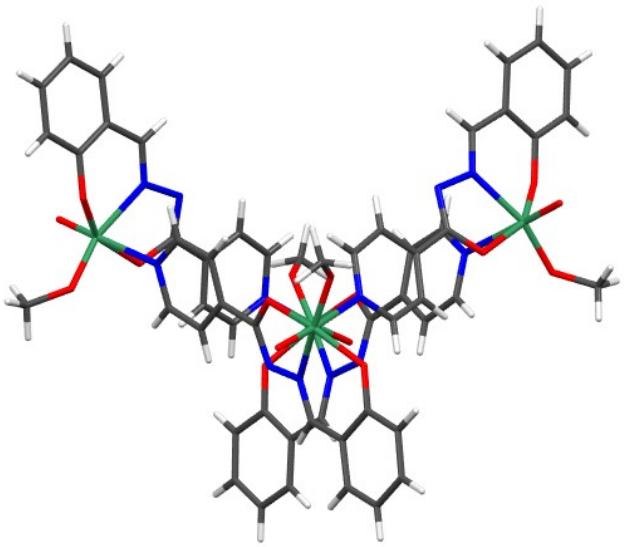

Fig. S7 Folded-square shape of tetranuclear complex **1t** (side view).

1.3. UV-Vis

Table S3 UV-Vis spectral data of H_2SIH and its complexes in methanol and acetonitrile.

Compound	Solvent	λ_{max}/nm (ε/dm^3 mol^{-1} cm^{-1})
H_2SIH	CH_3OH	214 ($1.88\cdot10^4$), ~238[a], ~279[a], 288 ($1.36\cdot10^4$), ~299[a], 333 ($1.17\cdot10^4$)
	CH_3CN	232 ($1.06\cdot10^4$), ~277[a], 286 ($1.69\cdot10^4$), 297 ($1.52\cdot10^4$), 329 ($1.24\cdot10^4$)
$[VO(SIH)(OCH_3)]_4$	CH_3OH	230 ($1.04\cdot10^5$), ~275[a], 322 ($6.95\cdot10^4$), 404 ($1.76\cdot10^4$)
	CH_3CN	231 ($7.37\cdot10^4$), 271 ($5.47\cdot10^4$), 323 ($4.27\cdot10^4$), ~340[a], 403 ($2.25\cdot10^4$)
$[VO(SIH)(OCH_3)]_n$	CH_3OH	231 ($3.18\cdot10^4$), ~275[a], 322 ($2.09\cdot10^4$), 404 ($5.78\cdot10^3$)
	CH_3CN	231 ($2.02\cdot10^4$), 267 ($1.66\cdot10^4$), 320 ($1.29\cdot10^4$), 390 ($5.25\cdot10^3$)
$[VO(SIH)(OC_2H_5)]_n$	CH_3OH	232 ($2.68\cdot10^4$), ~275[a], 322 ($1.82\cdot10^4$), 404 ($4.46\cdot10^3$)
	CH_3CN	231 ($1.27\cdot10^4$), 267 ($1.00\cdot10^4$), 320 ($7.89\cdot10^3$), 390 ($3.34\cdot10^3$)
$[VO(SIH)(OC_3H_7)]_n$	CH_3OH	231 ($2.78\cdot10^4$), ~275[a], 321 ($1.88\cdot10^4$), 404 ($4.67\cdot10^3$)
	CH_3CN	231 ($1.88\cdot10^4$), 267 ($1.54\cdot10^4$), 320 ($1.20\cdot10^4$), 390 ($4.89\cdot10^3$)
$[VO(SIH)(OC_4H_9)]_n$	CH_3OH	231 ($2.88\cdot10^4$), ~275[a], 322 ($1.95\cdot10^4$), 404 ($4.80\cdot10^3$)
	CH_3CN	231 ($2.13\cdot10^4$), 267 ($1.74\cdot10^4$), 320 ($1.36\cdot10^4$), 390 ($5.59\cdot10^3$)
$[VO(SIH)(OC_5H_{11})]_n$	CH_3OH	231 ($2.54\cdot10^4$), ~275[a], 322 ($1.71\cdot10^4$), 404 ($4.27\cdot10^3$)
	CH_3CN	231 ($2.50\cdot10^4$), 267 ($2.05\cdot10^4$), 320 ($1.60\cdot10^4$), 390 ($6.59\cdot10^3$)
$[VO_2(HSIH)]$[b]	CH_3OH	229, ~275[a], 322, 401
	CH_3CN	232, ~275[a], 323, ~338[a], 405

[a] Shoulder.
[b] Due to incomplete dissolution of the compound, ε values remained undetermined.

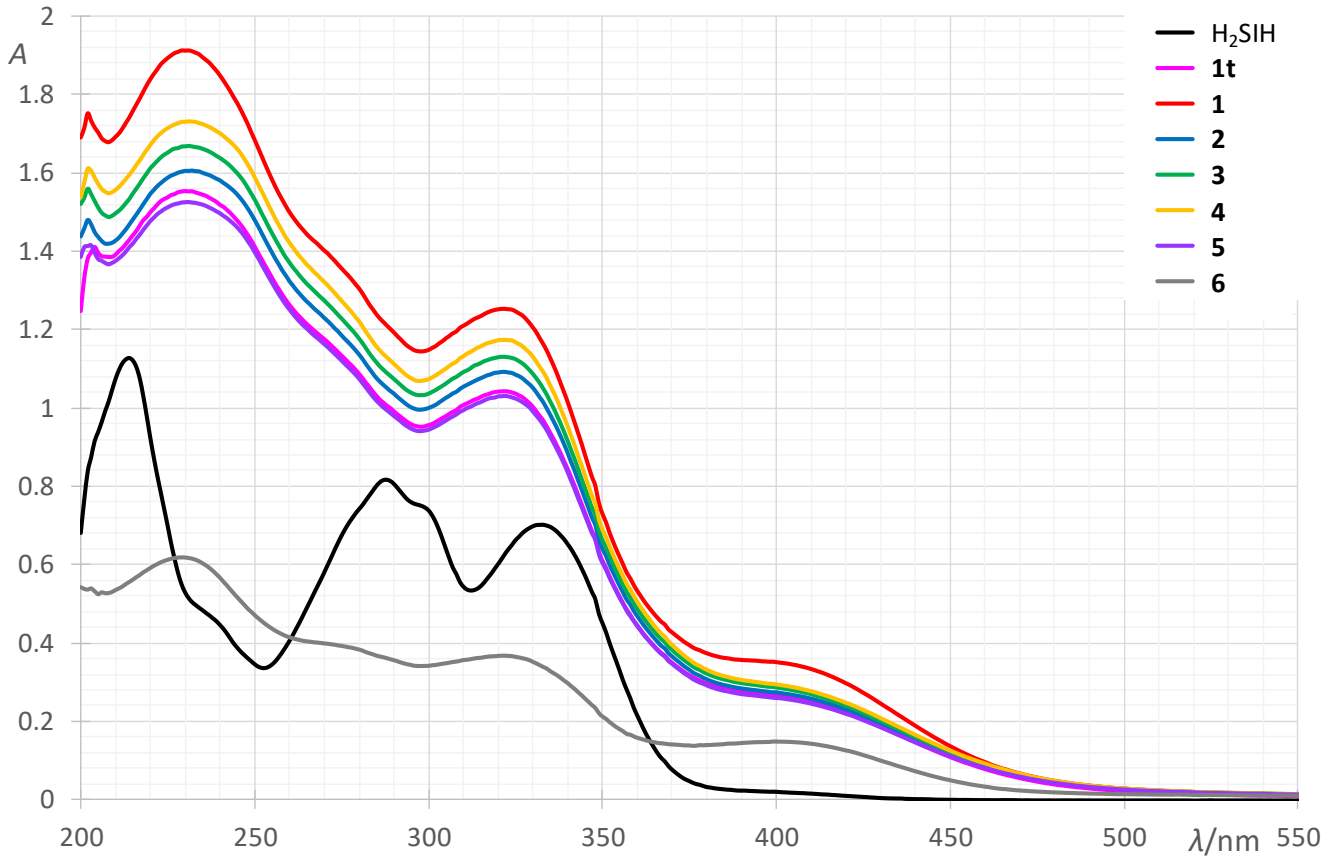

Fig. S8 The UV-Vis spectra of H_2SIH and its complexes in methanol. The concentrations were 6.0 × 10^{-5} mol dm^{-3} for H_2SIH and $[VO(SIH)(OR)]_n$ complexes (**1**–**5**), 1.5 × 10^{-5} mol dm^{-3} for $[VO(SIH)(OCH_3)]_4$ (**1t**), and below 3 × 10^{-5} mol dm^{-3} for $[VO_2(HSIH)]$ (**6**).

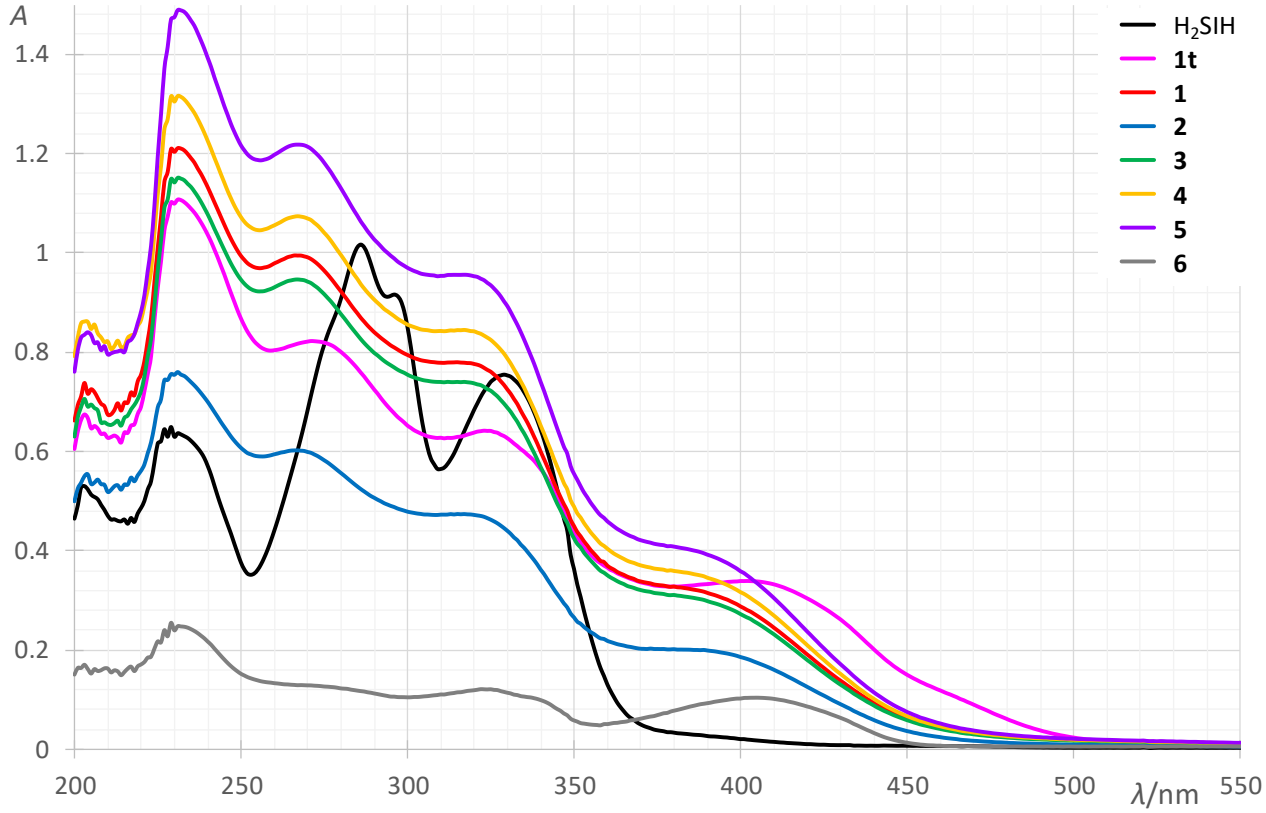

Fig. S9 The UV-Vis spectra of H_2SIH and its complexes in acetonitrile. The concentrations were 6.0 × 10^{-5} mol dm^{-3} for H_2SIH and $[VO(SIH)(OR)]_n$ complexes (**1**–**5**), 1.5 × 10^{-5} mol dm^{-3} for $[VO(SIH)(OCH_3)]_4$ (**1t**), and below 3 × 10^{-5} mol dm^{-3} for $[VO_2(HSIH)]$ (**6**).

1.4. NMR spectroscopy

Table S4 ^{1}H and ^{13}C chemical shifts (ppm) of H_2SIH and $[VO(SIH)(OC_3H_7)]$

Atom	H_2SIH		$[VO(SIH)(OC_3H_7)]$	
	δ / ppm (^{1}H)	δ / ppm (^{13}C)	δ / ppm (^{1}H)	δ / ppm (^{13}C)
1	8.56	151.41	8.84	154.41
4	–	162.51	–	169.32
5	–	140.92	–	139.94
6	7.90	121.76	8.07	122.41
7	8.76	149.75	8.68	149.27
8	–	–	–	–
9	8.76	149.75	8.68	149.27
10	7.90	121.76	8.07	122.41
11	–	117.99	–	120.18
12	–	158.21	–	164.20
13	6.95	116.34	7.04	116.45
14	7.33	131.83	7.55	134.52
15	6.94	119.24	6.96	102.14
16	7.48	130.33	7.65	132.60

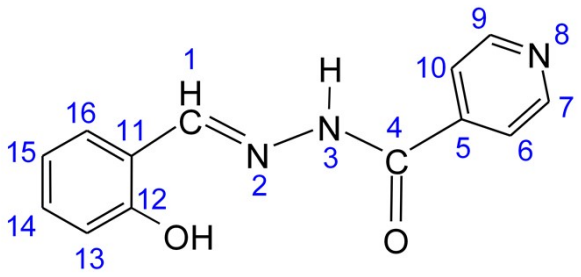

Scheme S1 The structural formula of H_2SIH with the NMR numbering scheme.

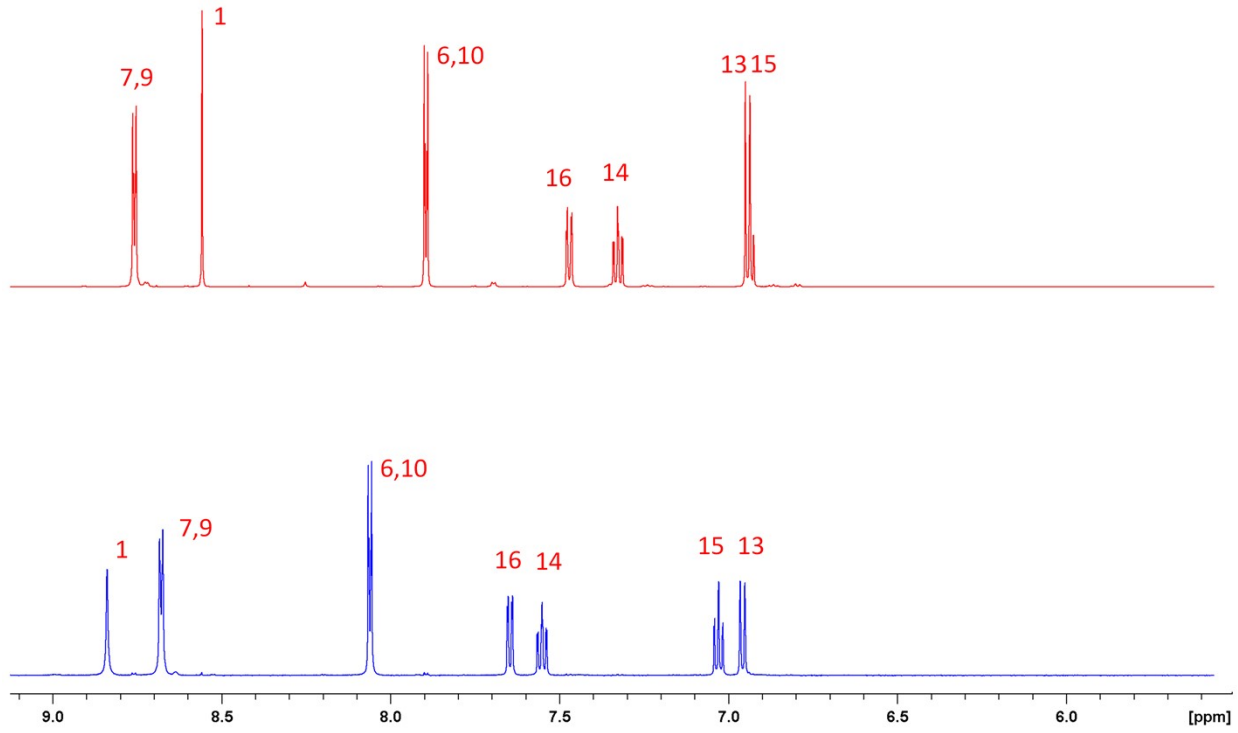

(a)

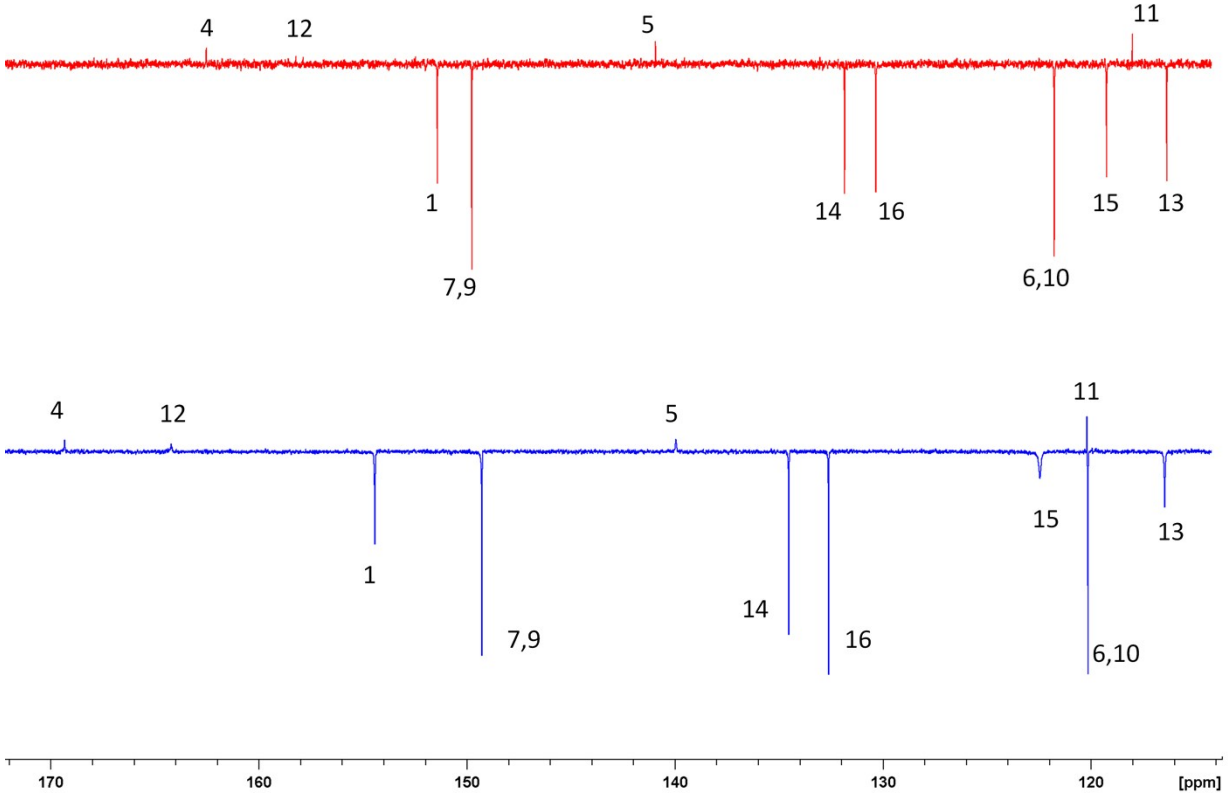

(b)

Fig. S10 A portion of the (a) ^{1}H NMR and (b) ^{13}C NMR spectra in CD_3OD of H_2SIH (red line), $[VO(SIH)(OC_3H_7)]$ (blue line).

1.5. ATR-IR spectroscopy

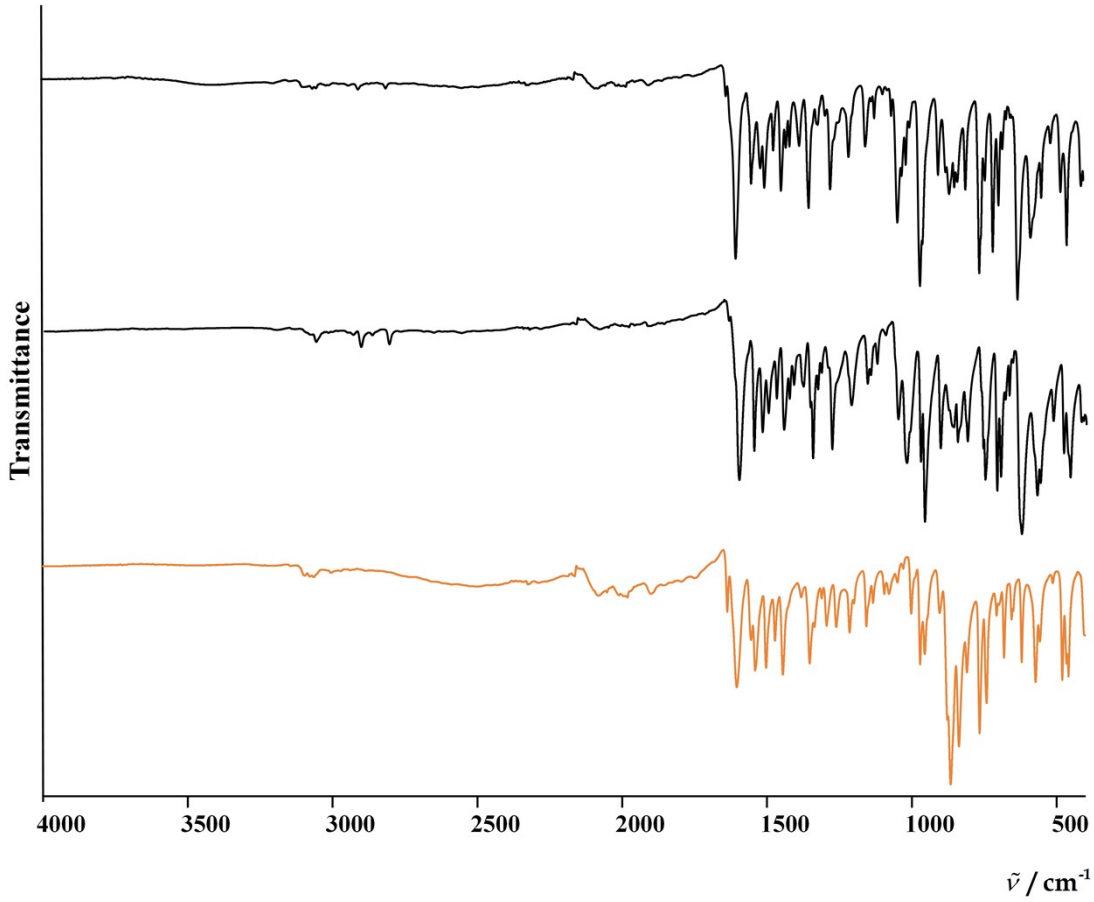

Fig. S11 IR-ATR spectra of $[VO(SIH)(OCH_3)]_4 \cdot 4CH_3OH$ (for **1t**·$4CH_3OH$), $[VO(SIH)(OCH_3)]_n \cdot 0.25MeOH$ (**1**·$0.25CH_3OH$) and $[VO_2(HSIH)]$ (**6**) (from top to bottom).

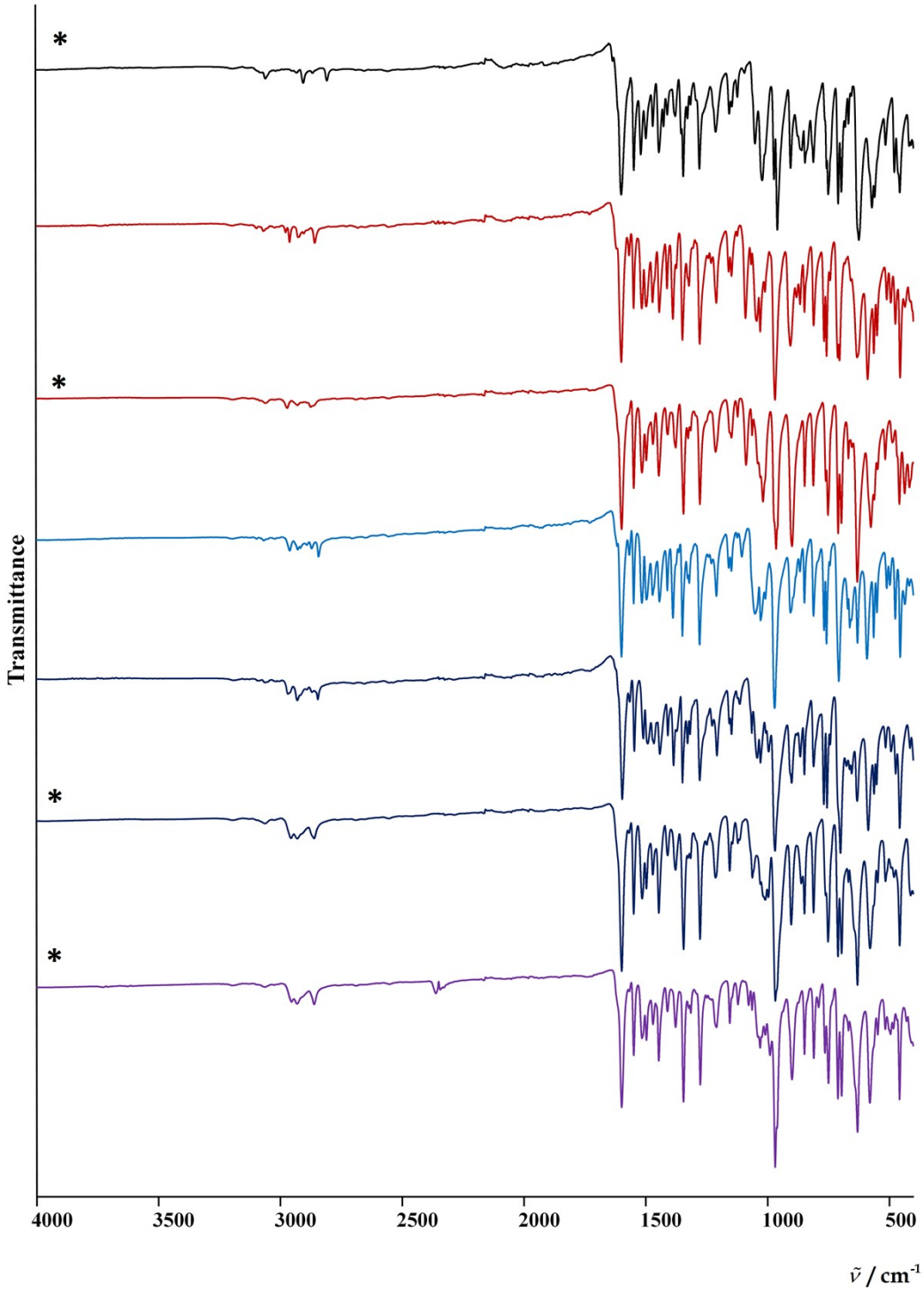

Fig. S12 IR-ATR spectra of coordination polymers (compounds belonging to the **β** series are marked with an asterisk): $[VO(SIH)(OCH_3)]_n$·0.25MeOH (**1β** ·0.25CH_3OH), $[VO(SIH)(OC_2H_5)]_n$ (**2α**), $[VO(SIH)(OC_2H_5)]_n$·0.25C_2H_5OH (**2β**·0.25C_2H_5OH), $[VO(SIH)(OC_3H_7)]_n$ (**3α**), $[VO(SIH)(OC_4H_9)]_n$ (**4α**), $[VO(SIH)(OC_4H_9)]_n$ (**4β**), $[VO(SIH)(OC_4H_9)]_n$ (**5β**) (from top to bottom).

1.6. TGA

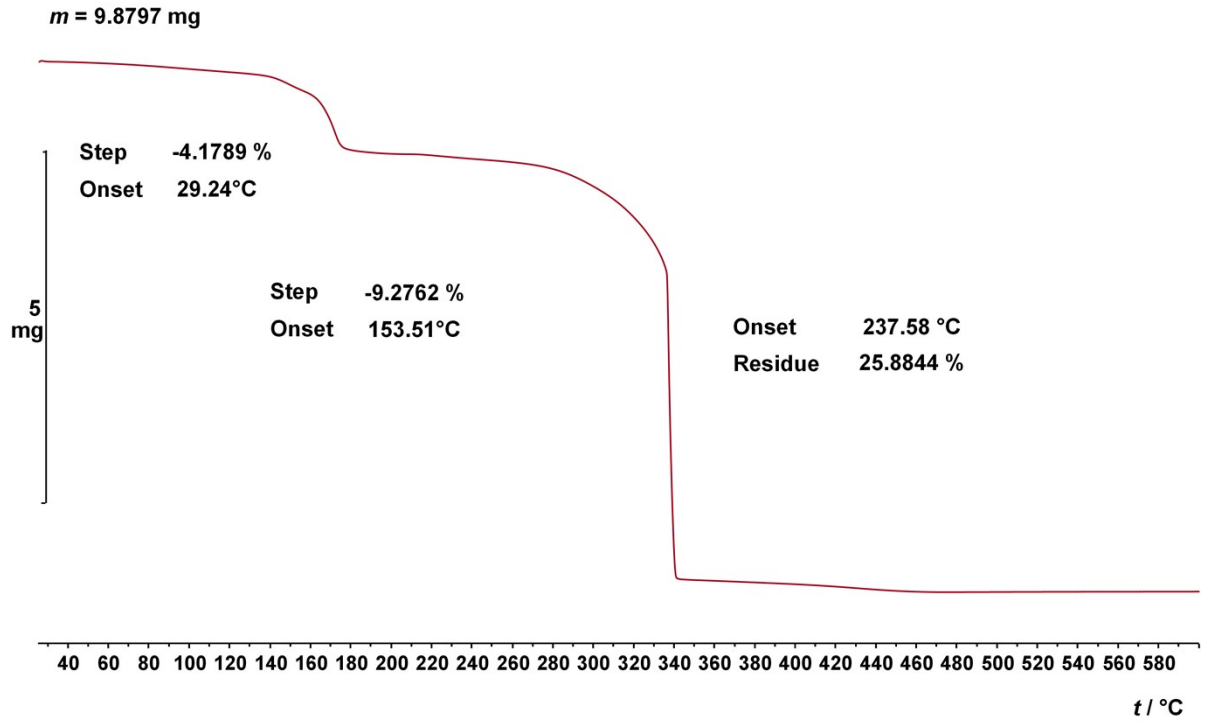

Fig. S13 TG curve of $[VO(SIH)(OCH_3)]_4 \cdot 2MeOH$ (**1t**·$2CH_3OH$) under the O_2 atmosphere in the range of 25 - 600 °C. Experiment was recorded with a heating rate of 5 °C min^{-1} in a dynamic atmosphere with a flow rate of 200 cm^3 min^{-1}.

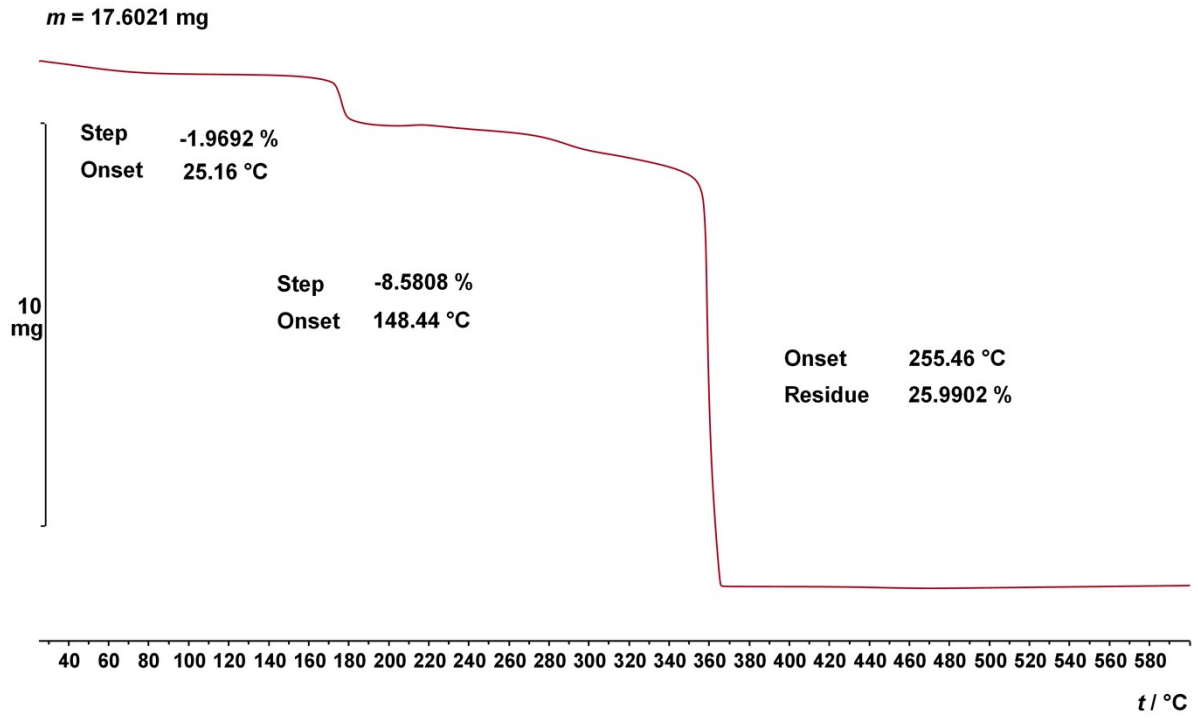

Fig. S14 TG curve of **1β**·0.25 CH_3OH under the O_2 atmosphere in the range of 25 - 600 °C. Experiment was recorded with a heating rate of 5 °C min^{-1} in a dynamic atmosphere with a flow rate of 200 cm^3 min^{-1}.

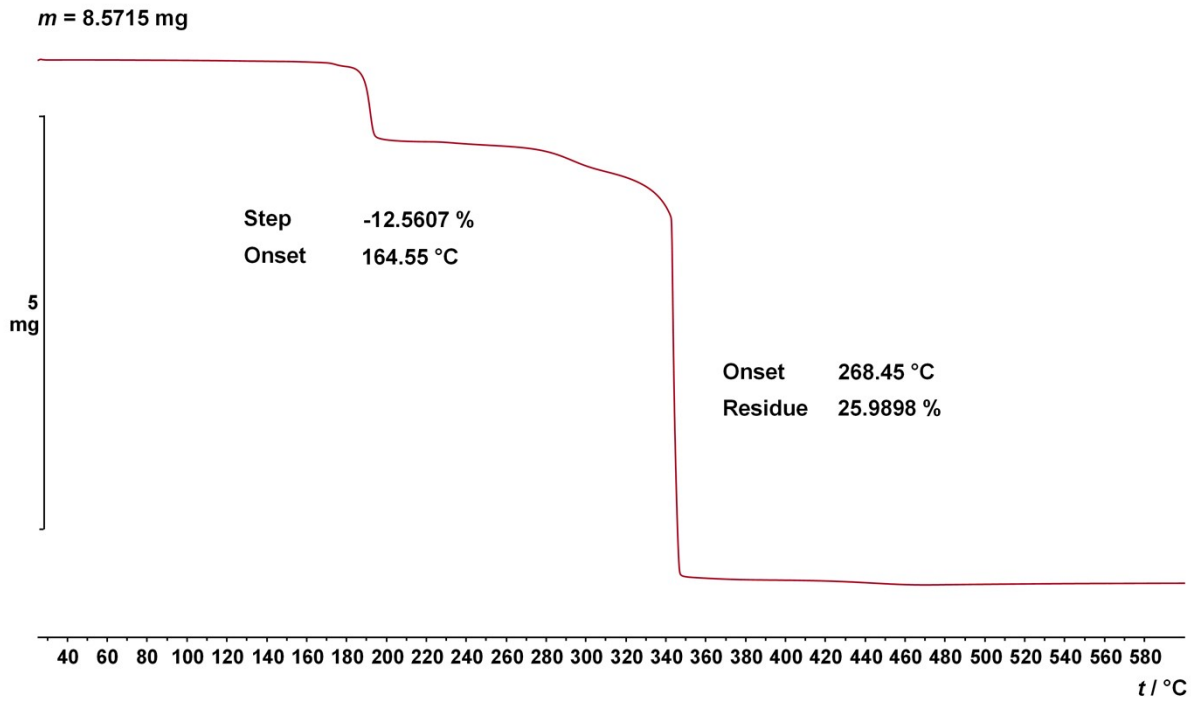

Fig. S15 TG curve of **2α** under the O_2 atmosphere in the range of 25 - 600 °C. Experiment was recorded with a heating rate of 5 °C min^{-1} in a dynamic atmosphere with a flow rate of 200 cm^3 min^{-1}.

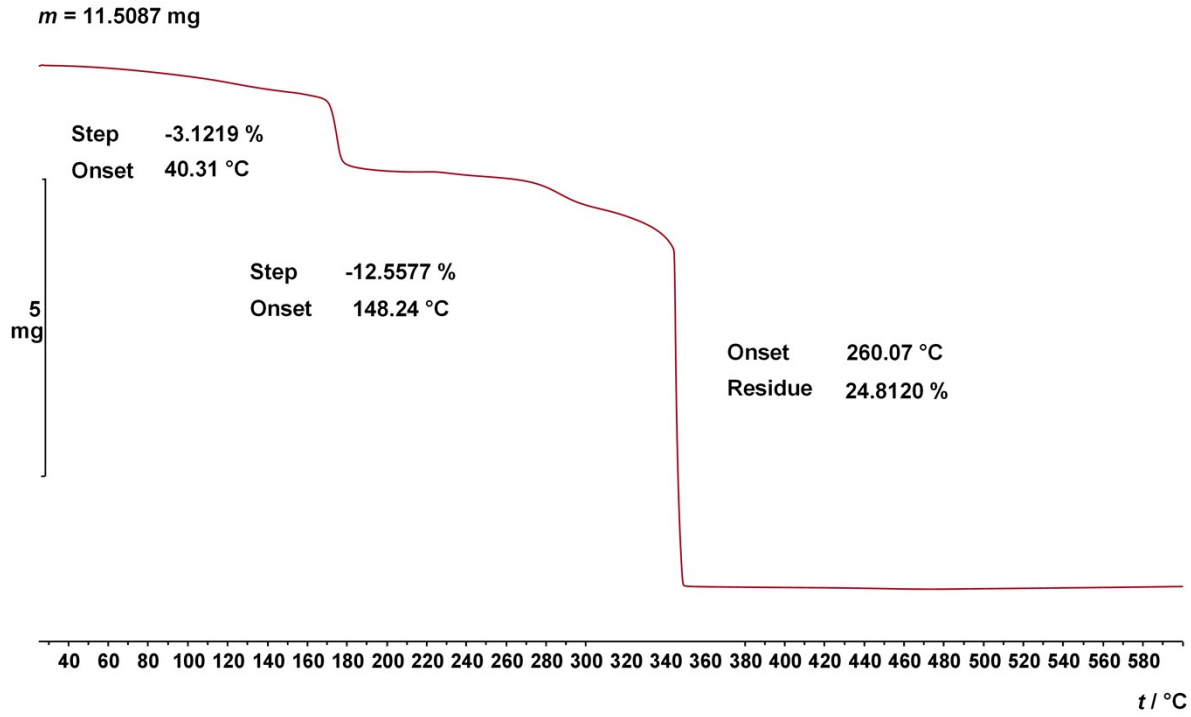

Fig. S16 TG curve of **2β**·0.25CH_3OH under the O_2 atmosphere in the range of 25 - 600 °C. Experiment was recorded with a heating rate of 5 °C min^{-1} in a dynamic atmosphere with a flow rate of 200 cm^3 min^{-1}.

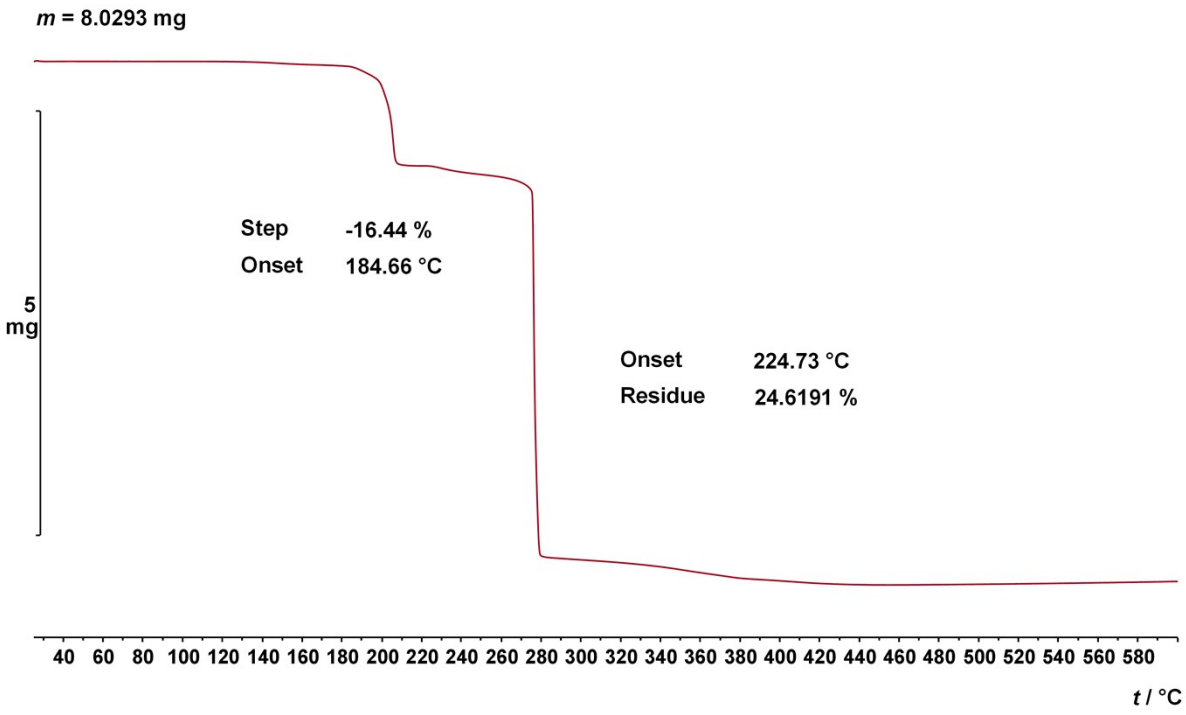

Fig. S17 TG curve of **3α** under the O_2 atmosphere in the range of 25 - 600 °C. Experiment was recorded with a heating rate of 5 °C min^{-1} in a dynamic atmosphere with a flow rate of 200 cm^3 min^{-1}.

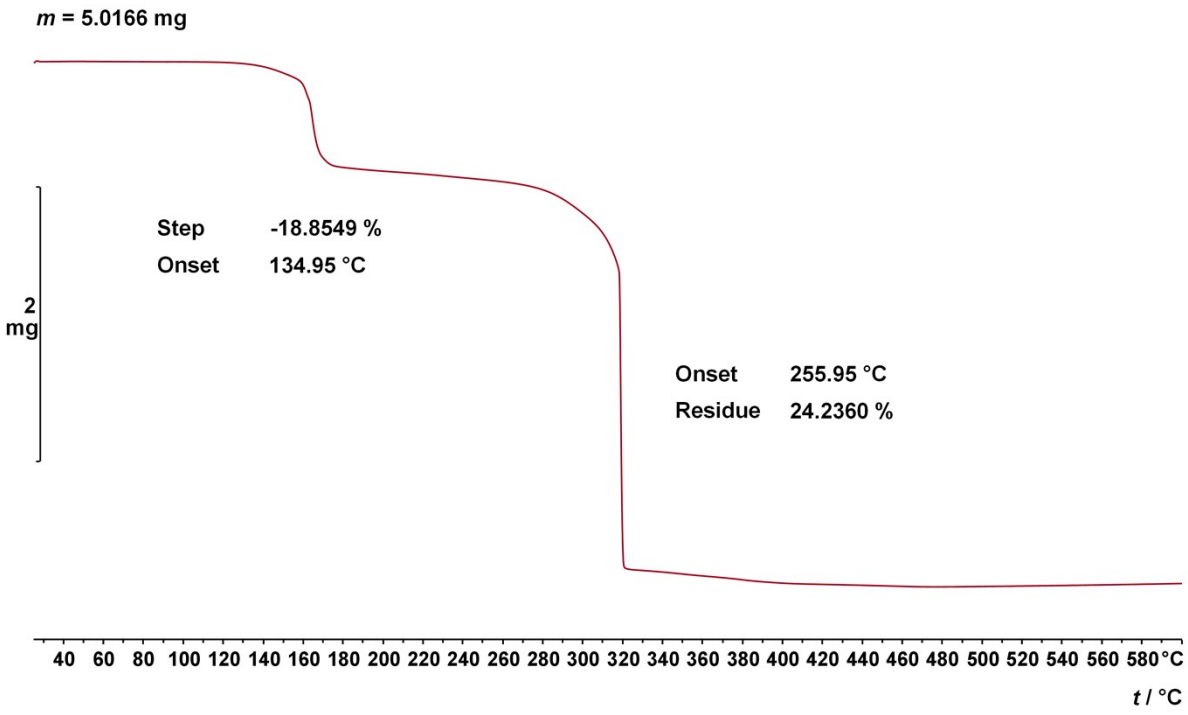

Fig. S18 TG curve of **4α** under the O_2 atmosphere in the range of 25 - 600 °C. Experiment was recorded with a heating rate of 5 °C min^{-1} in a dynamic atmosphere with a flow rate of 200 cm^3 min^{-1}.

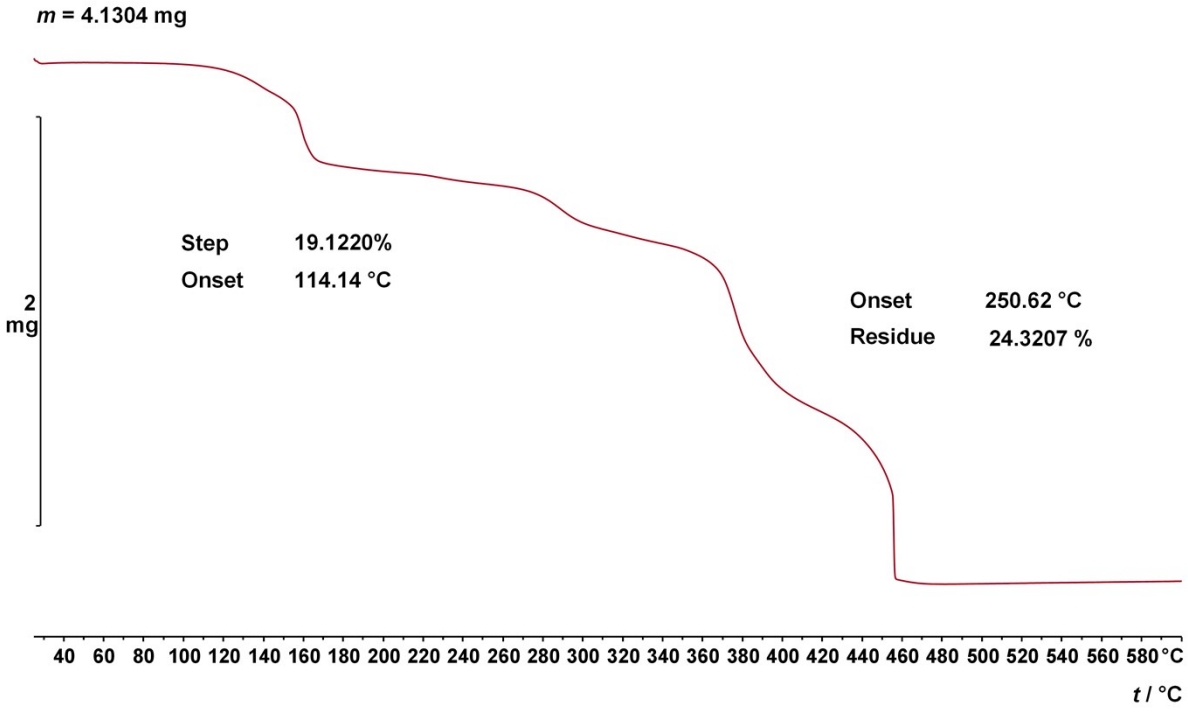

Fig. S19 TG curve of **4β** under the O_2 atmosphere in the range of 25 - 600 °C. Experiment was recorded with a heating rate of 5 °C min^{-1} in a dynamic atmosphere with a flow rate of 200 cm^3 min^{-1}.

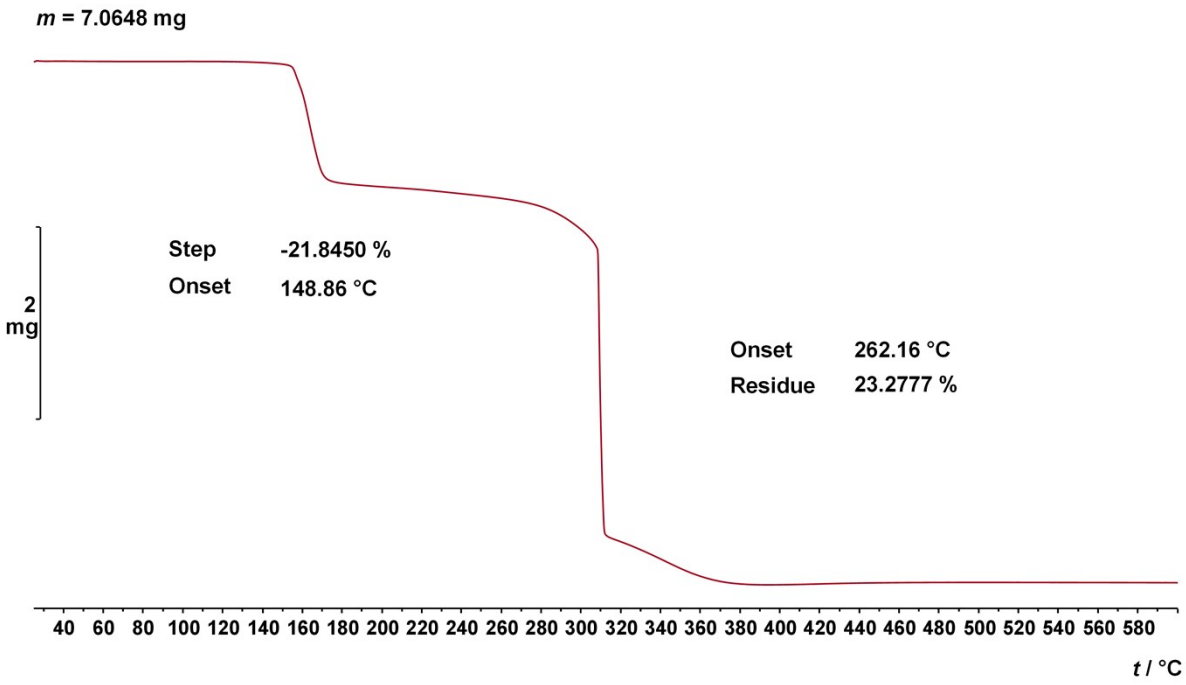

Fig. S20 TG curve of **5β** under the O_2 atmosphere in the range of 25 - 600 °C. Experiment was recorded with a heating rate of 5 °C min^{-1} in a dynamic atmosphere with a flow rate of 200 cm^3 min^{-1}.

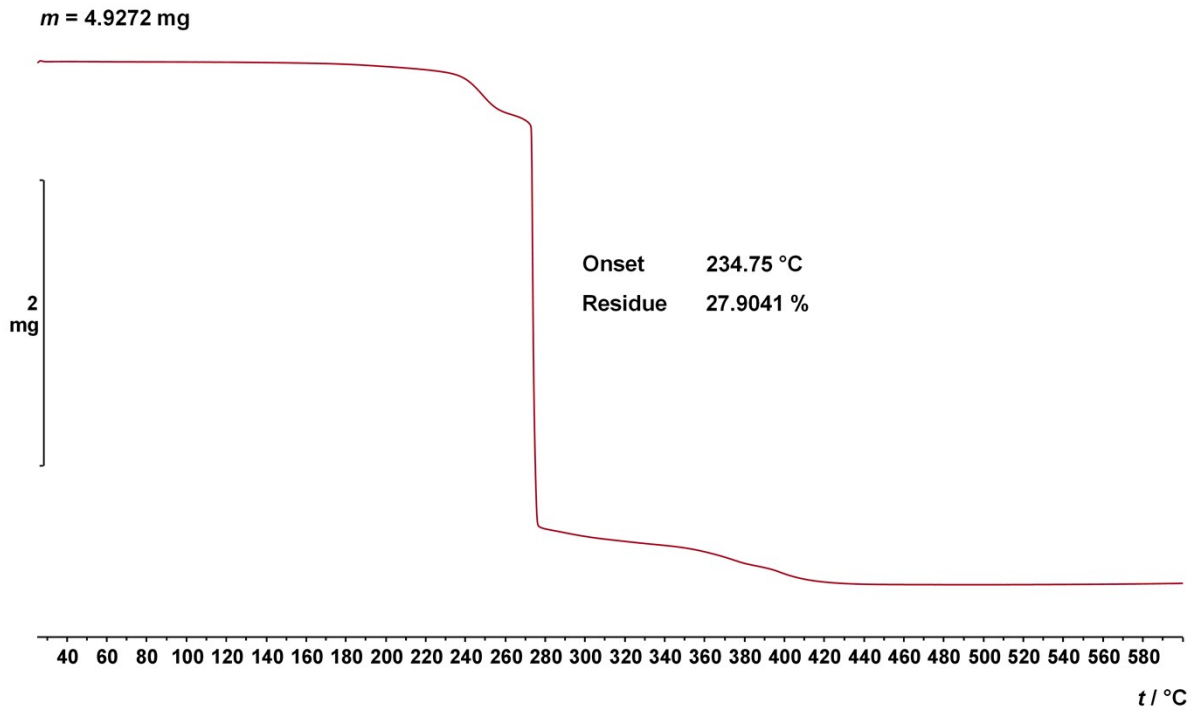

Fig. S21 TG curve of **6** under the O_2 atmosphere in the range of 25 - 600 °C. Experiment was recorded with a heating rate of 5 °C min^{-1} in a dynamic atmosphere with a flow rate of 200 cm^3 min^{-1}.

References

[1] T. Degen, M. Sadki, E. Bron, U. König, G. Nénert, The High Score suite. Powder Diffr. 2014, **29**, S13–S18. https://doi.org/10.1017/s0885715614000840

[2] Rigaku Oxford Diffraction. CrysAlisPro Software System, Version 1.171.42.49; Rigaku Oxford Diffraction: Oxford, UK, 2020.

[3] G. M. Sheldrick, SHELXT– Integrated space-group and crystal-structure determination. *Acta Crystallogr. A Found. Adv.* **2015**, 71, 3–8. doi:10.1107/s2053273314026370

[4] G. M. Sheldrick, Crystal structure refinement with SHELXL. *Acta Crystallogr. C Struct. Chem*. 2015, **71**, 3–8. doi:10.1107/s2053229614024218.

[5] O. V. Dolomanov, L. J. Bourhis, R. J. Gildea, J. A. K. Howard, Puschmann, H. OLEX2: a complete structure solution, refinement and analysis program. *J. Appl. Crystallogr.* **2009**, 42, 339-341. doi: 10.1107/s0021889808042726.

[6] A. L. Spek, Structure validation in chemical crystallography. *Acta Crystallogr. D Biol. Crystallogr.* **2009**, 65, 148–155. doi:10.1107/s090744490804362x.

[7] C. R. Groom, I. J. Bruno, M. P. Lightfoot, S. C. Ward, The Cambridge Structural Database. *Acta Crystallogr. B Struct. Sci. Cryst. Eng. Mater.* **2016**, 72, 171-179. doi:10.1107/s2052520616003954